Article

Not peer-reviewed version

Experimental Investigation on the Corrosion Detectability of A36 Low Carbon Steel Used in Multi-bolted Connections by the Method of Phased Array Corrosion Mapping

Jan Lean Tai , Rafał Grzejda * , Mohamed Thariq Hameed Sultan * , Andrzej Łukaszewicz * , Farah Syazwani Shahar , Wojciech Tarasiuk , Arkadiusz Rychlik

Posted Date: 29 June 2023

doi: 10.20944/preprints202306.2120.v1

Keywords: Phased Array Ultrasonic Testing (PAUT); Non-destructive Testing (NDT); Ultrasonic Thickness Gauge (UTG); multi-bolted connections; flat bottom hole; elevated temperature

Article

Experimental Investigation on the Corrosion Detectability of A36 Low Carbon Steel Used in Multi-Bolted Connections by the Method of Phased Array Corrosion Mapping

Jan Lean Tai [1], Rafał Grzejda [2]*, Mohamed Thariq Hameed Sultan [1, 3, 4, *], Andrzej Łukaszewicz [5,*], Farah Syazwani Shahar [1], Wojciech Tarasiuk [5] and Arkadiusz Rychlik [6]

[1] Department of Aerospace Engineering, Faculty of Engineering, Universiti Putra Malaysia, 43400 UPM Serdang, Selangor, Malaysia;
[2] Faculty of Mechanical Engineering and Mechatronics, West Pomeranian University of Technology in Szczecin, 19 Piastow Ave., 70-310 Szczecin, Poland;
[3] Laboratory of Biocomposite Technology, Institute of Tropical Forest and Forest Product (INTROP), University Putra Malaysia, 43400 UPM Serdang, Selangor, Malaysia;
[4] Aerospace Malaysia Innovation Centre [944751-A], Prime Minister's Department, MIGHT Partnership Hub, Jalan Impact, 63600 Cyberjaya, Selangor Darul Ehsan, Malaysia;
[5] Institute of Mechanical Engineering, Faculty of Mechanical Engineering, Bialystok University of Technology, 15-351 Bialystok, Poland;
[6] Faculty of Technical Sciences, University of Warmia and Mazury in Olsztyn, 10-719 Olsztyn, Poland.
* Corresponding author – rafal.grzejda@zut.edu.pl (RG); thariq@upm.edu.my (MTHS); a.lukaszewicz@pb.edu.pl (AL)

Abstract: Petrochemical plants use on-stream inspection more often to detect and monitor the corrosion on the equipment and piping system. Compared to ultrasonic thickness gauging and pulse-echo A-scan, phased array corrosion mapping has better coverability and can scan a large area to detect general and localized corrosion. This paper's objective is to obtain documentary evidence on the accuracy of corrosion detection from 30°C to 250°C on A36 low-carbon steel by carrying out simulation experiments every 10°C steps. A minimum of three sets of phased array corrosion mapping data in each temperature were collected to study and evaluate the detectability. The data evidence could enhance the confidence level of the plant's end users to use the phased array mapping in the future during an inspection. The experiments were found to be insufficiently thorough despite addressing the initial concerns, leaving more area for discussion in further studies, such as expanding the investigation to thicker carbon steel, stainless steel, and wedge materials.

Keywords: Phased Array Ultrasonic Testing (PAUT); Non-destructive Testing (NDT); Ultrasonic Thickness Gauge (UTG); multi-bolted connections; flat bottom hole, elevated temperature

1. Introduction

The existing petrochemical plants use on-stream inspection more often to detect and monitor the corrosion on the equipment and piping system typically built with multi-bolted connections [1,2]. Corrosion that occurs on the walls of the pipeline can affect the deformation of the connections and change the tension in the bolts, similar to the way pipes bend [3]. Any such change in bolt tension can in turn cause dangerous leakage of the fluid being transported. This is why adequate bolt tension is so important in flanged pipe connections [4,5].

On-stream inspection is a plant's maintenance system that monitors and assesses throughout plant operation; the benefit of on-stream inspection includes extending the turnaround time because some essential problem advancement may be monitored while the plant is operating.

One of the most crucial approaches is Condition Based Maintenance (CBM). CBM policy is based on data collected through condition monitoring. CBM's primary purpose is to prevent breakdowns and malfunctions by monitoring essential equipment component parts [6].

The purpose of condition monitoring is to inspect various petrochemical equipment such as storage tanks, pressure vessels, and piping systems [7] without shutting down the plants. Many different types of NDT methods/techniques can perform condition monitoring, but four factors should be considered when choosing an inspection method: 1. What kind of damage was the targeted mechanism, 2. What is the size of the targeted defect, 3. Where is the defect located, and 4. The inspection method sensitivity and limitations [8]. For example, if the targeted defect is located in the inner shell of the equipment with no external access or an operating temperature, the inspection results may be invalid. The condition monitoring location (CML) is the place chosen to assess the remaining thickness on the potential corrosion location regularly, often by ultrasonic thickness measurement to detect the wall loss.

Wagh demonstrates the advantage of employing RBI evaluation rather than the standard remaining life calculation to evaluate the above-ground storage tank and process piping in the petrochemical plant's remaining life [9]. The RBI is calculated based on the type of incident and the consequences if equipment fails, as well as the likelihood that the incident will occur; for example, the likelihood of new equipment failure until some period may be negligible, so no shutdown inspection for the equipment is required during this period.

An inspection manager computer software based on the RBI methodology was created to assist in the selection of response actions to unplanned events resulting in the release of hazardous materials. The RBI approach is frequently used to identify important equipment where inspection will provide the greatest benefit in terms of reducing operational risk. The costs connected with accidents are complex, especially when human life and deformed environments are involved, which presents a substantial obstacle in the decision-making process [10].

The damage mechanism is chosen based on several parameters, including the material composition of the equipment, the nature of the fluid treated or stored in the equipment, the surrounding processing environment, and other elements that influence the screening of damage criteria. By taking these elements into account, one can determine the exact types of damage processes that are likely to occur in the equipment. This information is required for successful inspection and maintenance procedures to prevent equipment deterioration or failure [11].

Liquid hydrocarbons, dissolved gases, water, and salts compose crude oil. It exists in the form of an emulsion, with water droplets scattered inside the continuous hydrocarbon phase. Natural gas, on the other hand, is a gas mixture of hydrocarbons, nitrogen, carbon dioxide, sulphur dioxide, water, and trace amounts of mercury, organic acids, and inert gases. Corrosive substances such as CO2, H2S, H2O, mercury, and organic acids can cause metal corrosion in the oil and gas sector throughout various stages of natural gas production, separation, processing, transportation, handling, and storage [12].

Carbon dioxide generates a type of corrosion known as sweet corrosion. Sour corrosion happens when H2S causes corrosion. O2 corrosion is referred to as oxygen corrosion. H2S can cause general and pitting corrosion, as well as hydrogen attack. Cracks and blisters are indicators of further growth. Human death and environmental damage can arise from the leakage of H2S into the environment through fissures.

The appearance of oxygen corrosion is pitting. Oxygen corrodes carbon steel, low alloy steels, copper, and its alloys. However, oxygen is required to keep protective oxide coatings on stainless steel, titanium, and aluminium in place.

The corrosion rate increases as the temperature rises. The solubility of hazardous gases, on the other hand, diminishes with increasing temperature. Temperature and corrosion rate have a complicated relationship. When the temperature reaches a particular point, the corrosion rate accelerates. The corrosion rate reduces when the solubility of corrosive gases in aqueous solutions diminishes after a certain temperature. When the temperature is low, H2S speeds up corrosion. These

 doi:10.20944/preprints202306.2120.v1

phenomena are particularly dangerous in view of the turbulent nature of the flow occurring under certain conditions in pipelines [13,14].

According to Wang and Yang, corrosion accounts for almost 80% of overall petrochemical plant failures. They emphasise that for every 10°C increase in temperature, the corrosion rate increases by 1-3 times. Furthermore, increasing pressure can increase the solubility of corrosive gases, hastening the corrosion process. These studies illustrate the importance of temperature and pressure in petrochemical plant corrosion rates [15]. Managing and reducing corrosion through appropriate material selection, protective coatings, and corrosion control techniques is critical to ensuring the integrity and reliability of petrochemical equipment and infrastructure.

Corrosion is a localised electrochemical oxidation and reduction reaction that occurs on metal surfaces. It consists of an anode, a cathode, and an aqueous solution or electrolyte containing positively and negatively charged ions with conductivity. Electrons are moved from the metal surface to another site during the electrochemical corrosion process, resulting in slow deterioration and eventual failure of the metal [16].

Internal corrosion is caused by gases or liquids that are stored or moved within the system. Corrosion can occur in both anaerobic (oxygen-free) and aerobic (oxygen-containing) conditions when metals are continuously exposed to these fluids. This continuous exposure to fluids causes corrosion, jeopardising the integrity and function of metal structures. To limit the effects of corrosion and preserve the longevity of metal components in various industrial contexts, preventive measures such as corrosion-resistant materials, protective coatings, and good maintenance practices are required.

Carbon steel corrosion is a serious problem in many chemical processing industries, including fire protection networks. Despite the advent of alternative piping materials, carbon steel remains a popular choice for the transportation of chemicals, acids, hydrocarbon products, and water due to its adaptability and low cost [17].

Corrosion can cause a gradual decrease in the wall thickness of carbon steel pipes over time. This reduction in thickness causes greater hoop stress, both throughout the pipe and in specific regions. As the hoop stresses interact mechanically with the pipe wall, they can cause expansion, buckling, deformation, and even rupture.

While welding defects, stress corrosion cracking, and hydrogen cracking can all cause major damage to pipes, they have not been shown to directly affect pipe wall thickness. These concerns, however, can contribute to total pipe degradation and jeopardise the integrity of carbon steel piping systems. To limit the impact of corrosion and guarantee the safe and dependable operation of carbon steel piping networks, preventative measures such as regular inspection, maintenance, and corrosion management techniques must be used [18].

General corrosion, also known as uniform corrosion, happens when a metal loses electrons due to electron flow to the cathode of the same metal. It is a common type of corrosion that affects the entire surface of the metal uniformly. Corrosion in general can occur in a variety of settings, including those containing chlorides, sulphides, and carbon dioxide, and can affect the faster wear of various parts of machinery and equipment [19,20].

The presence of chlorides, sulphides, and carbon dioxide in the crude distillation overhead system can lead to the development of general corrosion. These corrosive substances affect the system's metallic structure, creating a slow weakening of the metal. The general corrosion assault might cause a loss in the thickness of the metallic structure over time [21]. Preventive methods, including the use of corrosion-resistant materials, the application of protective coatings, frequent inspection and maintenance, and appropriate corrosion control strategies, can be applied to mitigate general corrosion in such systems. The impact of general corrosion can be reduced by following these steps, ensuring the safe and efficient operation of the crude distillation overhead system.

Pitting corrosion, also known as localised corrosion or pinhole corrosion, is a type of corrosion that has a small diameter but an excessive depth. Pitting pits arise on a microscopic size and cause metals and alloys to fail via perforation and stress corrosion cracking, among other modes of failure. Pitting can be classified into three stages: nucleation, growth and passivation, and sound stage

pitting. Pitting is influenced by material microstructure, chemical content, grain size, temperature, corrosive media, and pH [22]. Localised corrosion is more damaging than uniform corrosion, accelerating the initiation of corrosion leaks [23]. Corrosion can lead to corrosion cracking or stress corrosion cracking that can break the piping material [24,25].

Z. G. Zhang et al. present a nondestructive testing (NDT) approach for performing inspections during plant operation in a high-temperature environment. Thermal imaging, ultrasonic testing, and pulsed eddy current are examples of high-temperature-capable techniques [26]. The use of ultrasonic thickness gauging (UTG) to identify plant corrosion during plant operation can check up to 200°C. However, different technicians' and equipment's uncertainty may not be accurate at the same UTG point.

Ultrasonic testing is most commonly applied to on-stream inspection compared to other non-destructive tests mainly because of the lightweight equipment that provides greater accessibility in the complex petrochemical plant's environment. The test only requires accessing one side of the material surface, and it is non-radiation hazardous and can work with other trade workers around simultaneously.

Compared to other ultrasonic inspection techniques, such as ultrasonic thickness gauging, and pulse-echo A-scan, phased array corrosion mapping has better coverability.

Turcotte, Rioux, and Lavoie investigated tank corrosion mapping examination using conventional UT, PAUT, and 3D scanners. Unlike conventional UT beams, which only report one thickness at a time, phased array scans can produce a variety of thicknesses. One of the primary advantages of employing a phased array for corrosion mapping is that it functions in the same way as a conventional UT probe array, with all probes aligned with precise overlap and working concurrently. The size and number of probe elements, in addition to frequency, are the primary drivers [27].

In terms of time and coverage, the PAUT has an advantage over conventional ultrasonic thickness measurement. With conventional ultrasonic thickness measurement, it takes 2.7 hours to cover the 100mm x 100mm grid with a 1mm grid, assuming one second for each measurement step. The same area can be covered in a matter of seconds with phased array corrosion mapping [28].

PAUT can scan a large area to detect general and localized corrosion [29], but still faces the same ultrasonic inspection limitation that exceeds the standard recommended ultrasonic testing temperature of 52° [30] when carrying out on-stream corrosion monitoring at some piping operating temperatures above 200°C.

So far, there is still uncertainty in applying phased array corrosion mapping on high-temperature material surfaces. It can be seen that some petrochemical plant end users are concerned about what temperature the detection can reach. Some practitioners will answer affirmatively by saying a specific temperature can be achieved. Still, the further question is, how will the sensitivity change at such a high temperature? Currently, there is no detailed answer, mainly because there is no apparent reliable data.

To the best of the author's knowledge, currently, only Turcu et al. conducted phased array corrosion mapping up to 150°C by using Dual Linear Probe and reported that the challenge faced included the ultrasound velocity change when the temperature rises and the type of couplant and scanner selection but with limited result discussion and presentation [31].

This paper aims to obtain documentary evidence on how accurate the phased array corrosion mapping detectability can be from 30°C to 250°C on low carbon steel by conducting simulation experiments every 10°C steps. The data evidence could enhance the confidence level of petrochemical plants' end users to use phased array corrosion mapping in the future during an on-stream inspection to reduce petrochemical plants' downtime due to inspection.

Detailed experiment sequence will be discussed in the next section, including identification of the test specimen materials, test specimen design and fabrication, elevate temperature simulation, test equipment selection, and the testing procedure.

 doi:10.20944/preprints202306.2120.v1

The samples used in the test were A36 low-carbon steel plates, with a length of 200 mm × width of 100 mm × thickness of 15 mm. Machining slots of different depths represent general corrosion, and flat-bottom holes of different depths and diameters represent localised corrosion.

At least 3 sets of phased array corrosion mapping data were collected from the experimental test at 30°C to 250°C, with a difference of 10°C in each step. The carbon steel plate was heated by a heating element and monitored with a thermocouple and hand-held thermometer with a temperature accuracy of +-0.5°C.

2. Methodology

The quantitative experiment began with handheld laser-induced breakdown spectroscopy to verify the low-carbon steel material grade. After that, designing the test specimen with detailed consideration and preparing the test specimen by machining took place. The simulation method to raise the material temperature and the testing procedure, including the equipment and accessories selection, are explained in this section.

2.1. Test Specimen

A test specimen constructed of low-carbon steel was employed in the study. Because of its advantageous qualities, this material grade is widely used in the petrochemical industry. The test specimen measured 200mm in length, 100mm in width, and 15mm in thickness. However, the original mill certificate or documentation that would normally identify the precise low-carbon steel grade of the item was lost during the experiment.

The types of technical operations are taken from the production engineer's dictionary [31]. A handheld laser-induced breakdown spectroscopy (LIBS) approach was used to evaluate the material grade and certify that it corresponded to A36 low-carbon steel. LIBS is an elemental analysis method that uses a laser beam to produce a tiny plasma on the material's surface. The light released by the plasma is then analysed to establish the material's chemical makeup.

The author was able to confirm that the chemical composition of the test material matched the properties of A36 low-carbon steel by performing LIBS analysis on it. The previous stage was critical in ensuring the accuracy and reliability of the material following experiments and observations.

Material verification, such as handheld LIBS spectroscopy, is critical in research and industrial applications where an exact understanding of the material's composition and properties is necessary for accurate and reproducible results.

In the petrochemical industry, wall loss is classified as general corrosion with gradual wall loss and localized corrosion with isolated pit holes. Localized pits are hard to detect by ultrasonic thickness gauging because of the detected orientation and the probe size, but phased array corrosion mapping can have better detectability [32].

This study used the SolidWorks CAD system to produce the test specimen for the experiment [33,34]. They were able to create a three-dimensional (3D) model of the test specimen using computer-aided design software [35]. Figure 2a shows a 3D drawing prepared in a 1:1 ratio to ensure correctness and effective communication with the CNC milling process. Before fabricating the test specimen, the CAD system provided a diverse platform for designing and visualising it. This enabled the consideration of numerous parameters, such as the experiment's dimensions, shape, and unique features. They were able to make exact tweaks and modifications to guarantee the final test specimen fulfilled the desired parameters by working in a digital environment.

After the 3D drawing was completed, the CNC machining fabrication began. CNC machining is a manufacturing process that uses pre-programmed computer software to control the movement and functioning of machining equipment [36,37]. The SolidWorks 3D drawing acted as a blueprint for the CNC machining process, guiding the creation of the test specimen with high precision.

The combination of CAD design and CNC machining allowed for the accurate and efficient manufacture of the test specimen. This verified that the finished specimen matched the specified design, proportions, and features required for the experiment. The use of these modern technologies

Preprints (www.preprints.org) | NOT PEER-REVIEWED | Posted: 29 June 2023 doi:10.20944/preprints202306.2120.v1

improved the research process and contributed to the reproducibility and reliability of the experimental outcomes.

Therefore, both general and localized corrosion was considered in the specimen design to simulate the wall loss. Instead of a side drill hole [38], general corrosion was represented by a machining notch with a 5mm width and varying depths of 2mm, 4mm, 6mm, and 8mm. In comparison, localized corrosion is represented by flat bottoms holes (FBH) and varying diameters of 20mm, 15mm, 10mm, and 5mm from rolls with different depths of 3mm (20% wall loss) and 6mm (40% wall loss) for calibration and carryout experiment test [39]. Figure 1 gives the test specimen design with detailed dimensions, and Figure 2 contrasts the specimen 3D view and the fabricated test specimen by machining.

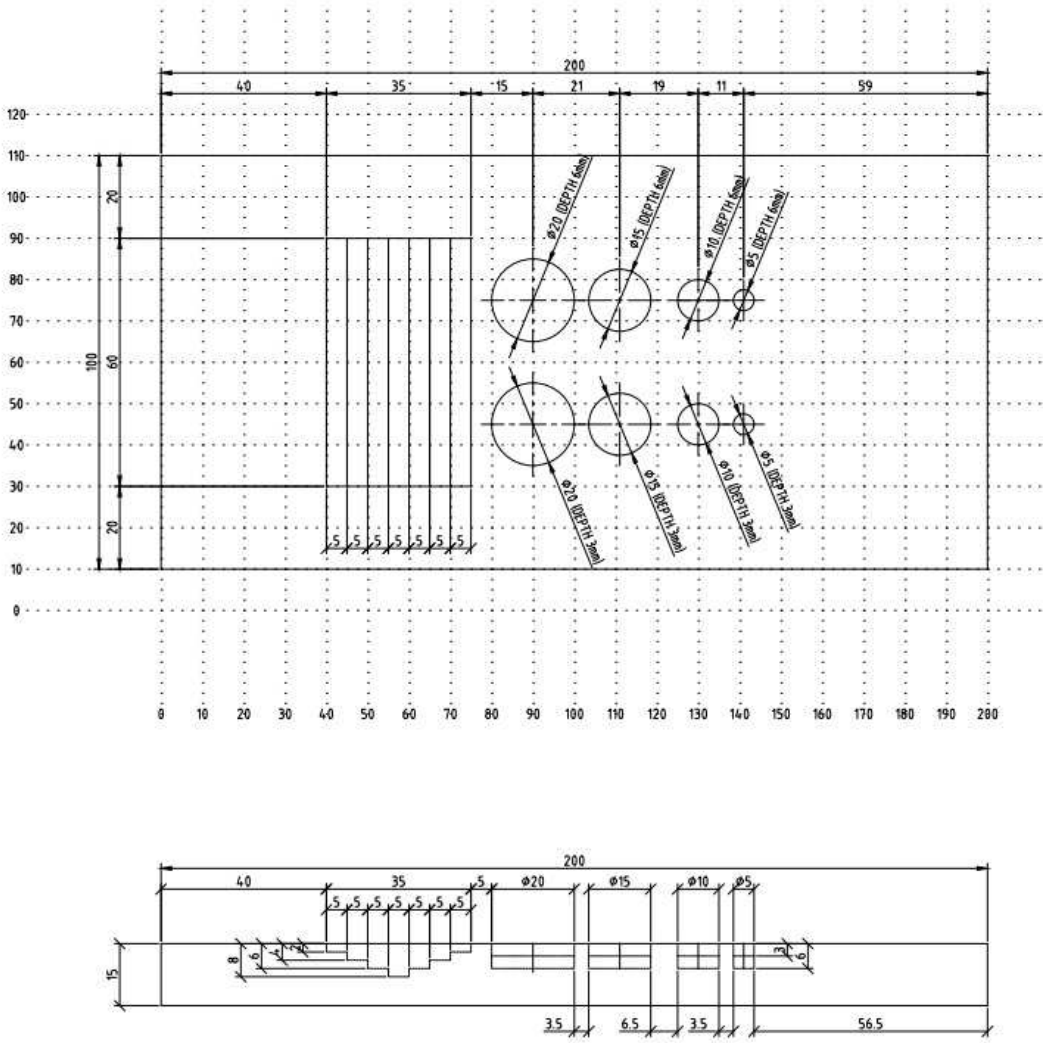

Figure 1. Experiment setup on A36 carbon steel material.

 doi:10.20944/preprints202306.2120.v1

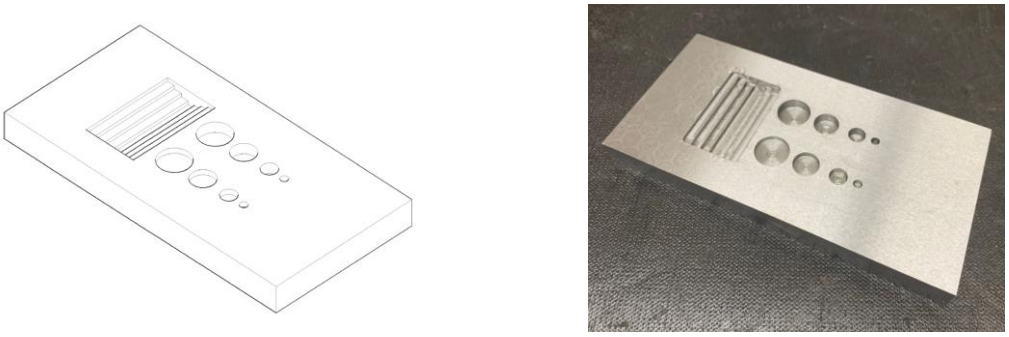

(**a**) (**b**)

Figure 2. (**a**) Test specimen 3D View; (**b**) Fabricated test specimen.

2.2. Elevated temperature simulation method

In order to successfully apply the phased array corrosion mapping for on-stream inspection, the experiment was conducted at temperatures ranging from 30°C to 250°C to simulate plant operating conditions. The carbon steel plate was placed on a ceramic pad heater element to heat from 30°C to 250°C, with a difference of 10°C in each step, and monitored with a thermocouple and hand-held thermometer with a temperature accuracy of +-0.5°C.

An experiment across a temperature range of 30°C to 250°C was carried out to assess the possibility of using phased array corrosion mapping for on-stream inspection in plant operating circumstances. The goal was to replicate the real operational conditions of the plant where the inspection would take place.

A carbon steel plate was placed on top of a ceramic pad heater element to accomplish this. The heating element aided in the progressive rise in temperature from 30°C to a high of 250°C. The temperature was raised in 10°C increments, allowing for a thorough evaluation of the phased array corrosion mapping technique at various temperature points.

Thermocouples were strategically placed on the top, middle, and bottom sections of the carbon steel plate to ensure exact temperature monitoring. Throughout the heating process, these thermocouples delivered precise temperature readings. A hand-held thermometer with a high degree of precision of 0.5°C was also employed as an extra way of temperature verification.

The authors were able to examine the effectiveness and dependability of the phased array corrosion mapping technique in a range of operational temperatures by running the experiment under controlled temperature circumstances and closely monitoring temperature changes. This data is critical for verifying the technique's applicability and performance in real-world settings with changing temperatures encountered during plant operations.

2.3. Phased array corrosion mapping

The difference between this experiment and the general phased array corrosion mapping is that the temperature of the surface temperature of the detected object is higher than the standard recommended temperature. Some challenges were encountered because it was not based on commonly known operating standards.

The first obstacle was the possibility of damaging the probe's piezo-element at extremely high surface temperatures. The probe's piezo element may be subjected to thermal stress as temperatures rise, resulting in degradation or even complete failure. This puts the quality and reliability of the ultrasound signals acquired throughout the inspection procedure in jeopardy [40,41]. It needed to take this into account and devise methods to reduce the influence of high temperatures on the probe's performance.

The nature of the ultrasonic couplant commonly utilised in phased array corrosion mapping posed the second challenge. The traditional couplant is water-soluble and evaporates quickly as the temperature rises. When the surface temperature of the test object surpasses 100°C, the functionality

 doi:10.20944/preprints202306.2120.v1

of the couplant is disrupted. Loss of the couplant can result in insufficient coupling between the probe and the test object, resulting in lower signal transmission and inspection accuracy [42,43].

Addressing these issues necessitated the development of novel solutions that were suited to the individual experimental conditions. Alternative materials or protective coatings, for example, might be investigated to improve the thermal resistance of the probe's piezo element, preserving its integrity even at high temperatures. Furthermore, selecting a suitable couplant or developing specialised high-temperature couplants capable of withstanding the extreme temperatures experienced during the inspection process would be required to maintain dependable coupling between the probe and the test object.

This study aimed to build a framework for conducting phased array corrosion mapping at higher surface temperatures, allowing for more effective on-stream inspection in industrial environments with heightened temperatures by recognising and overcoming these limitations.

Additionally, longitudinal velocity is obtained by measuring round-trip echo from the known material thickness [44]. An earlier experiment that successfully addressed the issue of how the temperature of the object being detected might affect the ultrasonic velocity was employed in this study. The earlier experiment verified the theoretical velocity calculation with include the heat-conduction coefficient K [45]. After considering the mentioned issues and conducting several trials, a preferable testing combination was ultimately discovered.

The testing uses a high-temperature-resistant wedge [46] and focuses on limiting contact time during detection, while the phased array probe uses a general-purpose 5L64 probe [47]. The water-soluble couplant is also replaced with high-temperature-resistant oil.

The process flow of this experiment can be summarised through several steps:

1. Determine the test specimen's base material grade and validate it with portable laser-induced breakdown spectroscopy. This stage confirms that the material composition satisfies the needed criteria, such as A36 low-carbon steel grade.
2. Select the temperature range to examine and refer to the velocity values. The velocity values can be estimated using the appropriate formulae and have been validated before with actual test results. It is well understood that velocity decreases with increasing temperature, and a reference list of velocity values ranging from 30°C to 250°C is given for comparison during the experiment [48].
3. Heat the test specimen to the specific experimental temperature. At the same time, calibrate the PAUT machine to the specified parameters.
4. The temperature of the test specimen is monitored using thermocouples strategically positioned. To ensure accuracy and reliability, temperature values are checked and confirmed with a thermal metre.
5. To obtain data from the machined slots and FBH, perform the PAUT test on the heated test specimen. To achieve excellent coverage and data capture, the phased array probes are precisely positioned and aligned.
6. Transfer the test data collected to a computer for interpretation and analysis. To process the data and provide visual representations of the corrosion mapping results, specialised software is employed.
7. Repeat steps 5–7 until at least three sets of data are gathered in each temperature range. This repeat enables data validation and statistical analysis to guarantee that the results are consistent and reliable.

3. Results and Discussion

The corrosion mapping data from the experiment can be classified into five separate stages based on the temperature range. The first step covers the temperature range of 30°C to 60°C. The velocity of the ultrasonic waves decreased as the temperature climbed throughout this period. However, the decibel (dB) levels remained rather constant, resulting in duplicated data with little variance. The successful identification of the machined slots that reflected general corrosion was one of the experiment's most significant features. These slots were created in a variety of depths, including 2mm, 4mm, 6mm, and 8mm. They have distinct and distinct edges that were seen in the corrosion

Preprints (www.preprints.org) | NOT PEER-REVIEWED | Posted: 29 June 2023 doi:10.20944/preprints202306.2120.v1

mapping data. To aid in the visualisation and interpretation of the corrosion extent, each depth was assigned a different colour.

These findings illustrate the utility of PAUT corrosion mapping in identifying and characterising corrosion at various depths. The unique colours provided for each depth level improve the visual depiction of corrosion features, allowing for exact assessment and analysis of corrosion extent.

The two rolls of different depth FBH that represent localized corrosion can be identified clearly in the 6mm depths (40% wall loss) roll in all the diameter sizes, the 3mm depths (20% wall loss) FBH is noted for 10mm, 15mm, and 20mm diameter can be identified clearly in sizes, but in the 5mm diameter FBH, the data can identify the indication but unable to present the round shape clearly. Figure 3 shows the phased array corrosion mapping data image at 50°C.

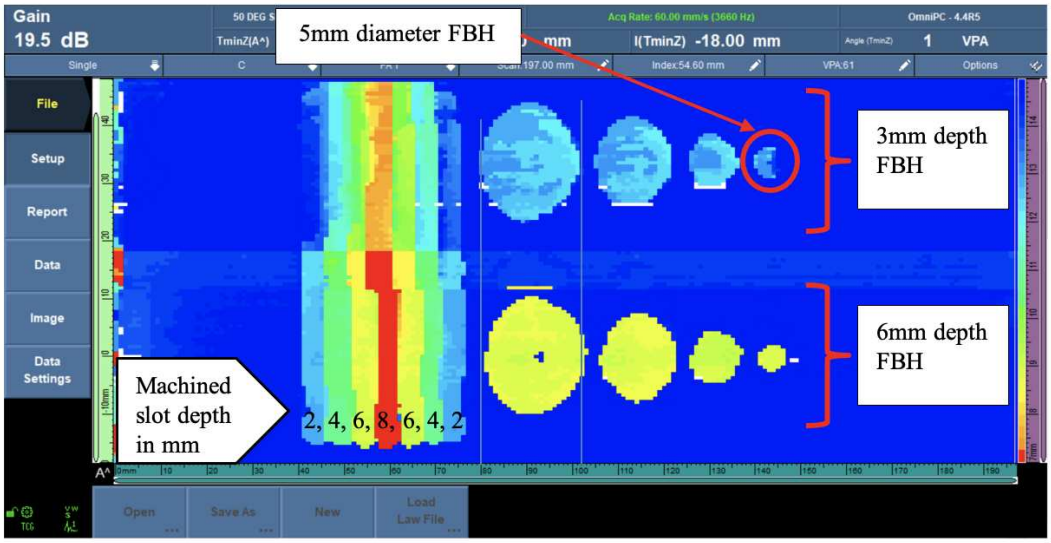

Figure 3. PAUT corrosion mapping data at 50°C.

The experiment's second stage covered a temperature range of 60°C to 100°C. During this stage, increasing the decibel (dB) level as the temperature rose was required to achieve an acceptable sensitivity level for corrosion detection. The data obtained in this stage was identical to the preceding group in that machined slots and flat-bottom holes (FBH) were discovered. However, only the 3mm depth (representing 20% wall loss) FBH did not clearly display the shape of the 5mm diameter FBH. Figure 4 shows the phased array corrosion mapping data image at 100°C.

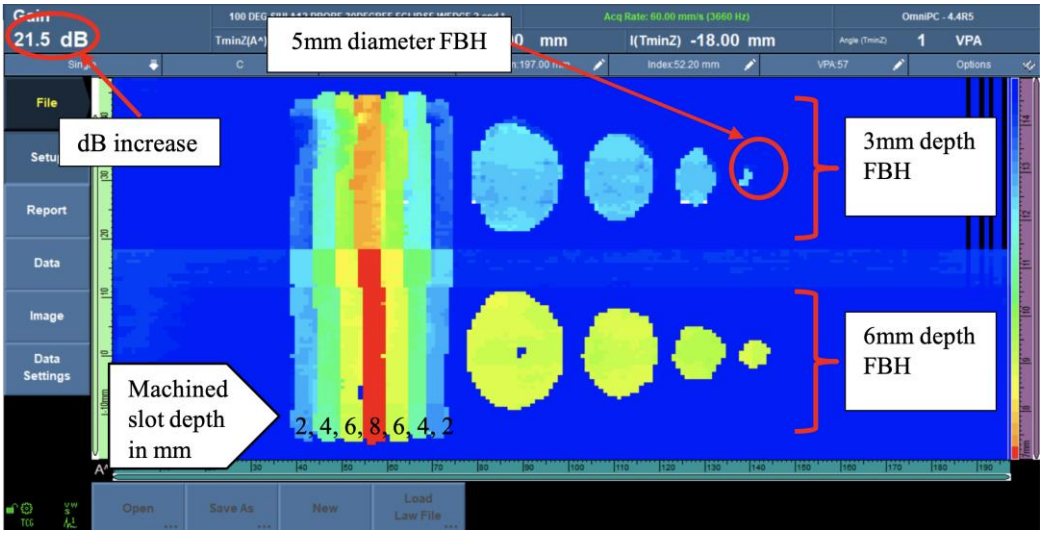

Figure 4. PAUT corrosion mapping data at 100°C.

Preprints (www.preprints.org) | NOT PEER-REVIEWED | Posted: 29 June 2023 doi:10.20944/preprints202306.2120.v1

In the third stage, due to the elevated temperature settings, particular measures had to be taken during the third stage of the experiment, which covered the temperature range of 100°C to 140°C. The scanning technique had to be carried out with greater caution because the couplant used in the method began to vaporise, causing smoke to appear. This created an impediment and challenge in gathering correct data. To solve these issues, it was critical to reduce scanning time. By shortening the scanning procedure, the heat transfer from the wedge to the probe's piezo element might be reduced, lowering the risk of probe damage.

Similar to the second stage, decibel level changes were required during the third stage to ensure ideal sensitivity levels. The observed velocity changes necessitated fine-tuning of the decibel settings. Despite the difficulties created by the elevated temperatures, the machined hole representing general corrosion could be clearly detected in all possible specified depths. The existence of a distinct edge in the data allowed for reliable corrosion detection and characterisation. It was noticed, however, that the 3mm depths (representing 20% wall loss) FBH data still had difficulties in showing the whole round shape of the 5mm diameter FBH.

In the following stage, with temperature ranging from 150°C to 180°C as Figure 5 shows, the machined slot images boundary lines at different depths begin to blur, and the display colour of the 2mm slot is the same as the colour of the material surface, making it difficult to distinguish. On the contrary, the 5mm diameter FBH could not be shown as round before showing signs of improvement.

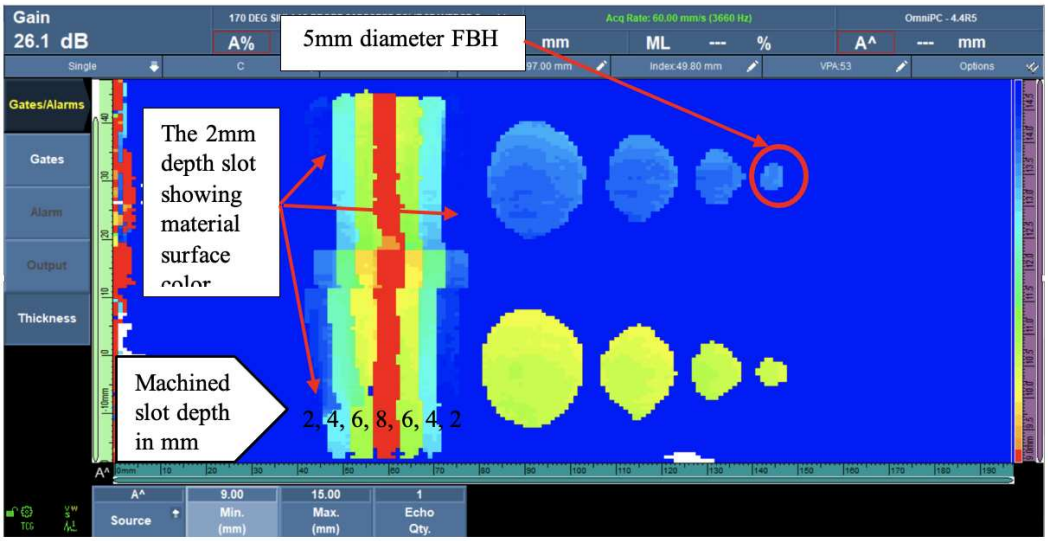

Figure 5. PAUT corrosion mapping data at 170°C.

The last stage of data is over 190°C and up to 250°C, where the data collection condition is more severe in this temperature range. The heat can be felt during scanning even while wearing insulated gloves. This procedure requires more accurate data acquisition to reduce the probe contact time. This stage also must have higher dB to maintain good imaging. The machined slot images in this stage can be identified except for the 8mm slot depth images unable to show the 5mm slot width. The two rolls of different depth flat bottom holes that represent localized corrosion can be identified clearly in both the 6mm depths (40% wall loss) and 3mm depths (20% wall loss) roll, except the middle of the diameter of 6mm roll FBH showing some uncaptured image shape. Still, it did not affect the overall result. Figure 6 shows the phased array corrosion mapping data image at 220°C.

Preprints (www.preprints.org) | NOT PEER-REVIEWED | Posted: 29 June 2023 doi:10.20944/preprints202306.2120.v1

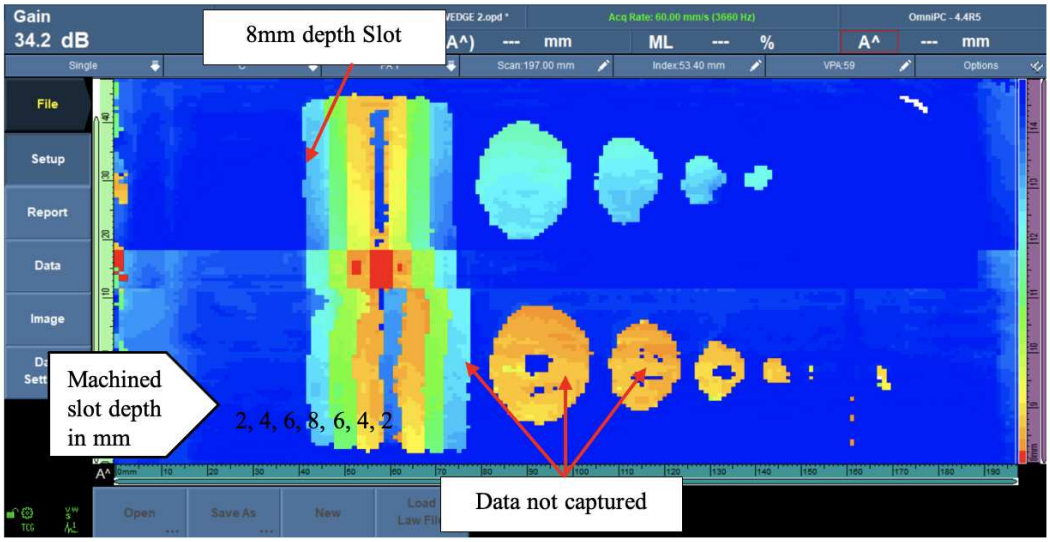

Figure 6. PAUT corrosion mapping data at 220°C.

4. Conclusions

This study aimed to collect a large amount of data in order to explore the efficacy of phased array corrosion mapping on low-carbon steel across a wide temperature range. A total of 72 data sets were methodically gathered, ranging from 30°C to 250°C at 10°C intervals. These comprehensive data sets were critical to meeting the project's objectives and providing valuable insights for this study.

The results of the phased array corrosion mapping experiment on low carbon steel at temperatures ranging from 30°C to 250°C revealed the detectability of corrosion in the given temperature range. However, it is crucial to note that this experiment may not have completely covered every possibility that could have occurred. The findings and debates offered in this article open up new possibilities for investigation and invite more in-depth examination and discussion.

The study's inadequacies or gaps present an opportunity for additional research and investigation. By filling these gaps, researchers will be able to gain a better understanding of the effectiveness and limitations of phased array corrosion mapping in a variety of temperature situations, material compositions, and equipment configurations. This article lays the groundwork for future research and urges the scientific community to participate in discussions and collaborative efforts to develop the field of ultrasonic inspection and corrosion mapping techniques, particularly in the field of multi-bolted jointed pipelines.

The experiment worked with a base metal thickness of 15mm in this study. Although this thickness was adequate to reflect the thicknesses of common pipe walls, it is important to note that thicker base metals may be used in subsequent tests to broaden the application area of phased array corrosion mapping's use in petrochemical plants. As a result, the technique might be applied to a broader range of equipment in such facilities [49].

The use of thicker base metal in future investigations is significant because of its effect on ultrasound attenuation. The attenuation of ultrasonic waves becomes more pronounced as the thickness of the material increases. As a result, exploring the combination of greater material thickness and high temperatures would be an ideal future research direction. It can acquire a more thorough understanding of the ultrasonic attenuation phenomenon by investigating thicker base metals and their behaviour under high-temperature settings. This knowledge would help to build more precise and dependable inspection strategies, allowing for effective corrosion mapping in various petrochemical plant equipment [50].

Extending the experiment to encompass thicker base metals and higher temperatures would increase the utility and versatility of phased array corrosion mapping in industrial settings. It would provide useful insights into the behaviour of different thicknesses of materials and aid in optimising the inspection procedure for enhanced corrosion detection and monitoring.

Although carbon steel is the most widely used in the petrochemical industry, other base materials must be addressed. For example, stainless steel [51] can be better resistant to corrosion and high pressure, and relatively require error-free. Otherwise, the consequences will be rather severe. Stainless steel is also the base material most likely to encounter stress corrosion cracking that would be beneficial for use in monitoring stream corrosion [52] and sliding contact temperature [53].

The material of the wedge is also a good direction for discussion. If it can be used without any risk of high temperatures and be in contact with for a longer time, it will bring more convenience and reduce overall inspection time.

The observation that the 5mm FBH cannot show a complete image at low temperatures but gets more clearly reflected at high temperatures implies that the object being tested has thermal tension. This discovery raises the possibility of additional discussion and investigation.

A major problem is an inability to detect minor faults while pipes are at room temperature during shutdown inspection. It means that under normal working settings, specific defects or imperfections may be more difficult to detect and diagnose. This emphasises the importance of inspecting at greater temperatures, which mirror actual working conditions and provide a more accurate depiction of the material's behaviour and the existence of flaws. Further investigation and discussion on the impact of thermal tension on ultrasonic testing and the detection of tiny defects could yield useful insights and advances in corrosion mapping techniques.

Following that, it is critical to discuss the current research findings with petrochemical plant end users in order to solicit their feedback and suggestions on the prospective use of the inspection design in real-life situations. Obtaining their comments is beneficial in determining the feasibility and practicability of incorporating the research findings into their ongoing projects. Engaging with end users will also provide insights into unique difficulties that may develop in the site context, allowing for further study extension.

Researchers can get a deeper understanding of the industry's objectives and restrictions by partnering with petrochemical plant end users, leading to the development of specialised inspection methodologies that are more effective and consistent with real-life circumstances. This collaboration will promote knowledge sharing and the development of best practices, ultimately leading to breakthroughs in inspection methodology and equipment selection.

Author Contributions: Conceptualization, data curation, formal analysis, investigation, methodology, visualization, and writing of the first draft were performed by Jan Lean Tai. Supervision and funding acquisition was made by Mohamed Thariq Hameed Sultan, Rafał Grzejda, Andrzej Łukaszewicz, Wojciech Tarasiuk and Arkadiusz Rychlik. Project administration was done by Farah Syazwani Shahar. Mohamed Thariq Hameed Sultan, Rafał Grzejda and Farah Syazwani Shahar reviewed and edited the previous versions of the manuscript. All authors read and approved the final manuscript.

Funding: The authors would like to thank Universiti Putra Malaysia for the financial support through Geran Inisiatif Putra Siswazah (GP-IPS) with grant number 9739200.

Data Availability Statement: All data generated or analysed during this study are included in this article.

Acknowledgements: The authors would also like to express their gratitude to the Department of Aerospace Engineering, Faculty of Engineering, Universiti Putra Malaysia, and the Laboratory of Biocomposite Technology, Institute of Tropical Forestry and Forest Product (INTROP), Universiti Putra Malaysia (HICOE) for their close collaboration in this study.

Conflicts of Interest: The authors have no competing interests to declare relevant to this article's content.

References

1. Grzejda, R. Thermal strength analysis of a steel bolted connection under bolt loss conditions. *Eksploatacja i Niezawodnosc – Maintenance and Reliability* **2022**, *24*, 269–274, doi:10.17531/ein.2022.2.8.
2. Grzejda, R.; Parus, A.; Kwiatkowski, K. Experimental studies of an asymmetric multi-bolted connection under monotonic loads. *Materials* **2021**, *14*, 2353, doi:10.3390/ma14092353.
3. Jaszak, P. Prediction of the durability of a gasket operating in a bolted-flange-joint subjected to cyclic bending. *Engineering Failure Analysis* **2021**, *120*, 105027, doi: 10.1016/j.engfailanal.2020.105027.
4. Jaszak, P. The elastic serrated gasket of the flange bolted joints. *International Journal of Pressure Vessels and Piping* **2019**, *176*, 103954, doi: 10.1016/j.ijpvp.2019.103954.

5. Grzejda, R.; Parus, A. Experimental studies of the process of tightening an asymmetric multi-bolted connection. *IEEE Access* **2021**, *9*, 47372-47379, doi:10.1109/ACCESS.2021.3067956.
6. Uchida, S.; Chimi, Y.; Kasahara, S.; Hanawa, S.; Okada, H.; Naitoh, M.; Kojima, M.; Kikura, H.; Lister, D.H. Improvement of Plant Reliability Based on Combining of Prediction and Inspection of Crack Growth Due to Intergranular Stress Corrosion Cracking. *Nuclear Engineering and Design* **2019**, *341*, 112–123, doi:10.1016/j.nucengdes.2018.10.021.
7. Jaszak, P.; Skrzypacz, J.; Borawski, A.; Grzejda, R. Methodology of leakage prediction in gasketed flange joints at pipeline deformations. *Materials* **2022**, *15*, 4354, doi:10.3390/ma15124354.
8. Dhandha, K.H. Shut down Inspection Requirements in Oil and Gas Refineries. *NDE 2020 - Virtual Conference & Exhibition* **2020**.
9. Wagh, P.V. Risk Based Inspection Approach for Effective Monitoring Remaining Life for Integrity of Refinery Equipment. *NDE 2018- Conference & Exhibition* **2018**.
10. Vianello, C.; Milazzo, M.F.; Maschio, G. The Management of Industrial Safety in Chemical and Petrochemical Industry by Comparing Costs and Benefits. *Chem Eng Trans* **2018**, *67*, 379–384, doi:10.3303/CET1867064.
11. Siswantoro, N.; Priyanta, D.; Ramadhan, J. Implementation of Risk-Based Inspection (RBI) in Condensate Separator and Storage Vessel: A Case Study. *International Journal of Marine Engineering Innovation and Research* **2021**, *6*, doi:10.12962/j25481479.v6i1.7565.
12. Groysman, A. Corrosion Problems and Solutions in Oil, Gas, Refining and Petrochemical Industry. *Koroze a Ochrana Materialu* **2017**, *61*, 100–117, doi:10.1515/kom-2017-0013.
13. Urbanowicz, K.; Zarzycki, Z. Improved lumping friction model for liquid pipe flow. *Journal of Theoretical and Applied Mechanics* **2015**, *53*, 295–305, doi: 10.15632/jtam-pl.53.2.295.
14. Urbanowicz, K. Modern modeling of water hammer. *Polish Maritime Research* **2017**, *24*, 68–77, doi: 10.1515/pomr-2017-0091.
15. Wan, Z.; Yang, J. Research on Corrosion Management Technology of Petroleum Pipeline and Pressure Vessel. *IOP Conf Ser Earth Environ Sci* **2021**, *692*, doi:10.1088/1755-1315/692/4/042057.
16. Jafar Mazumder, M.A. Global Impact of Corrosion: Occurrence, Cost and Mitigation. *Global Journal of Engineering Sciences* **2020**, *5*(4), doi:10.33552/gjes.2020.05.000618.
17. Sidun, P.; Łukaszewicz, A. Verification of Ram-Press Pipe Bending Process Using Elasto-Plastic FEM Model. *Acta Mechanica et Automatica* **2017**, *11*, 47–52, doi:10.1515/ama-2017-0007.
18. Subramanian, C. Localized Pitting Corrosion of API 5L Grade A Pipe Used in Industrial Fire Water Piping Applications. *Eng Fail Anal* **2018**, *92*, 405–417, doi:10.1016/j.engfailanal.2018.06.008.
19. Zmarzły, P. Multi-dimensional mathematical wear models of vibration generated by rolling ball bearings made of AISI 52100 bearing steel. *Materials* **2020**, *13*, 5440, doi: 10.3390/ma13235440.
20. Warzecha, M.; Michalczyk, K.; Machniewicz, T. A novel slotted cylinder spring geometry with an improved energy storing capacity. *Arabian Journal for Science and Engineering* **2022**, *47*, 15539–15549, doi: 10.1007/s13369-022-06692-x.
21. Fajobi, M.A.; Loto, R.T.; Oluwole, O.O. "crude Distillation Overhead System": Corrosion and Control. *J Phys Conf Ser* **2019**, *1378*, doi:10.1088/1742-6596/1378/4/042090.
22. Wang, F.; Shan, Q.; Zhang, F.; Lu, F.; Li, J.; Yu, T.; Qu, C. Pitting Corrosion Behavior of Metal Materials and Research Methods. *IOP Conf Ser Earth Environ Sci* **2021**, *651*, doi:10.1088/1755-1315/651/3/032039.
23. Du, L.; Wang, Q.; Li, X.; Yan, H. Cause Analysis and Suggestion on Corrosion Leakage of Pipe in Atmospheric and Vacuum Pressure Unit. *IOP Conf Ser Mater Sci Eng* **2020**, *711*, doi:10.1088/1757-899X/711/1/012015.
24. Surkov, Yu.P.; Rybalko, V.G.; Sycheva, T.S.; Usenko, V.F.; Ott, K.F.; Dolgov, I.A. Corrosion Cracking in Gas Pipelines. *Russian Journal of Nondestructive Testing* **2000**, *36*, 68–71, doi:10.1007/bf02759398.
25. Dolgov, I.A.; Sadrtdinov, R.A.; Gorchakov, V.A.; Surkov, Y.P.; Rybalko, V.G.; Novgorodov, D. v. Analysis of the Development of Stress Corrosion Cracking in Pipelines of Compressor Stations. *Russian Journal of Nondestructive Testing* **2008**, *44*, 68–75, doi:10.1134/S1061830908010099.
26. Zhang, Z.G.; Feng, H.X.; Zhao, W.H. The NDT Methods under High Temperature Service Environment. *MATEC Web of Conferences* **2016**, *40*, 1–3, doi:10.1051/matecconf/20164004001.
27. Turcotte, J.; Rioux, P.; Lavoie, J. Comparison Corrosion Mapping Solutions Using Phased Array , Conventional UT and 3D Scanners. *19th World Conference on Non-Destructive Testing 2016* **2016**, 1–10.
28. Ber, L. le; Benoist, G.; Dainelli, P. Corrosion Detection and Measurement Improvement Using Advanced Ultrasonic Tools. *19th World Conference on Non-Destructive Testing* **2016**, *554*, 1–8.
29. Bolotina, I.; Dyakina, M.; Kröning, M.; Mohr, F.; Reddy, K.M.; Soldatov, A.; Zhantlessov, Y. Ultrasonic Arrays for Quantitative Nondestructive Testing an Engineering Approach. *Russian Journal of Nondestructive Testing* **2013**, *49*, 145–158, doi:10.1134/S1061830913030030.
30. Jory, C. Tips for Internal Corrosion Using the Echo to Echo Technique with Compression. *The NDT Technician* **2019**, *18*.

31. Turcu, F.; Jedamski, T.; Treppmann, DR.D. In - Service Corrosion Mapping — Challenges for the Chemical Industry. *12th ECNDT* **2018**, 1–8.
32. Miatliuk, K.; Lukaszewicz, A.; Siemieniako, F. Coordination Method in Design of Forming Operations of Hierarchical Solid Objects. *2008 International Conference on Control, Automation and Systems, ICCAS 2008* **2008**, 2724–2727, doi:10.1109/ICCAS.2008.4694220.
33. Mohan, B.C.; Jeyasekhar, M.C.; Duhan, K.; Land, I.; Belait, K.; Manager, C. Oil and Gas Assets Condition Monitoring By High Sensitive PAUT Hydroform Corrosion Monitoring Technique for Integrity Assessment. *NDE 2019 - Conference & Exhibition* **2019**.
34. Łukaszewicz, A.; Miatliuk, K. Reverse Engineering Approach for Object with Free-Form Surfaces Using Standard Surface-Solid Parametric CAD System. *Solid State Phenomena* **2009**, *147–149*, 706–711, doi:10.4028/www.scientific.net/SSP.147-149.706.
35. Mircheski, I.; Lukaszewicz, A.; Trochimczuk, R.; Szczebiot, R. Application of CAX System for Design and Analysis of Plastic Parts Manufactured by Injection Moulding. *Engineering for Rural Development* **2019**, *18*, 1755–1760, doi:10.22616/ERDev2019.18.N463.
36. Lukaszewicz, A.; Panas, K.; Szczebiot, R. Design Process of Technological Line for Vegetables Packaging Using Cax Tools. *Engineering for Rural Development* **2018**, *17*, 871–876, doi:10.22616/ERDev2018.17.N494.
37. Lukaszewicz, A.; Szafran, K.; Jozwik, J. CAx Techniques Used in UAV Design Process. *2020 IEEE International Workshop on Metrology for AeroSpace, MetroAeroSpace 2020 - Proceedings* **2020**, 95–98, doi:10.1109/MetroAeroSpace48742.2020.9160091.
38. Mircheski, I.; Łukaszewicz, A.; Szczebiot, R. Injection Process Design for Manufacturing of Bicycle Plastic Bottle Holder Using CAx Tools. *Procedia Manuf* **2019**, *32*, 68–73, doi:10.1016/j.promfg.2019.02.184.
39. Jamil, J.; Yahya, S.Y.S. Corrosion Assessment Using Advanced Ultrasonic Measurement Technique. *IOP Conf Ser Mater Sci Eng* **2019**, *554*, doi:10.1088/1757-899X/554/1/012004.
40. Bazulin, E.G. The Calibration of an Ultrasonic Antenna Array Installed on a Wedge. *Russian Journal of Nondestructive Testing* **2014**, *50*, 227–238, doi:10.1134/S1061830914040020.
41. Kazys, R.; Vaskeliene, V. High Temperature Ultrasonic Transducers: A Review. *Sensors* **2021**, *21*, doi:10.3390/s21093200.
42. Cheong, Y.M.; Kim, K.M.; Kim, D.J. High-Temperature Ultrasonic Thickness Monitoring for Pipe Thinning in a Flow-Accelerated Corrosion Proof Test Facility. *Nuclear Engineering and Technology* **2017**, *49*, 1463–1471, doi:10.1016/j.net.2017.05.002.
43. Singh, K.J.; Matsuda, Y.; Hattori, K.; Nakano, H.; Nagai, S. Non-Contact Sound Velocities and Attenuation Measurements of Several Ceramics at Elevated Temperatures. *Ultrasonics* **2003**, *41*, 9–14, doi:10.1016/S0041-624X(02)00392-X.
44. Bazulin, E.G.; Sadykov, M.S. Determining the Speed of Longitudinal Waves in an Isotropic Homogeneous Welded Joint Using Echo Signals Measured by Two Antenna Arrays. *Russian Journal of Nondestructive Testing* **2018**, *54*, 303–315, doi:10.1134/S1061830918050029.
45. Łukaszewicz, A. Temperature Field in the Contact Zone in the Course of Rotary Friction Welding of Metals. *Materials Science* **2019**, *55*, 39–45, doi:10.1007/s11003-019-00249-4.
46. Slongo, J.S.; Gund, J.; Passarin, T.A.R.; Pipa, D.R.; Ramos, J.E.; Arruda, L.V.; Junior, F.N. Effects of Thermal Gradients in High-Temperature Ultrasonic Non-Destructive Tests. *Sensors* **2022**, *22*, 1–16, doi:10.3390/s22072799.
47. Kim, Y.L.; Cho, S.; Park, I.K. Analysis of Flaw Detection Sensitivity of Phased Array Ultrasonics in Austenitic Steel Welds According to Inspection Conditions. *Sensors* **2021**, *21*, 1–16, doi:10.3390/s21010242.
48. Van Thanh, P.; Thi Tuyet Nhung, P.; Thi Minh Thuy, L.; Hoa Nhai, N. Effect of Temperature on Ultrasonic Velocities, Attenuations, Reflection and Transmission Coefficients between Motor Oil and Carbon Steel Estimated by Pulse-Echo Technique of Ultrasonic Testing Method. *VNU Journal of Science: Mathematics-Physics* **2015**, *31*, 39–48.
49. Njelle, V.Z.; Ikeh, O.D.; E, I.A.; Usuoyibo, A. Study of Corrosion Rate of Low and Medium Carbon Steel Pressure Vessel in Nigeria Oil and Gas Industry Using Ultrasonic Testing (UT) and Phase Array Ultrasonic Testing (PAUT) Method. *Journal of Science and Technology Research* **2019**, *1*, 161–170.
50. Grzejda, R.; Kobielarz, M. Testing the mechanical properties of high-strength zinc-coated bolts: FEM approach. *Coatings* **2023**, *13*, 27, doi:10.3390/coatings13010027.
51. Krajewski, S.J.; Grochała, D.; Tomków, J.; Grzejda, R. Analysis of the surface stereometry of alloyed austenitic steel after fibre laser cutting using confocal microscopy. *Coatings* **2023**, *13*, 15, doi:10.3390/coatings13010015.
52. Siljama, O.; Koskinen, T.; Jessen-Juhler, O.; Virkkunen, I. Automated Flaw Detection in Multi-Channel Phased Array Ultrasonic Data Using Machine Learning. *J Nondestr Eval* **2021**, *40*, 1–13, doi:10.1007/s10921-021-00796-4.

53. Nosko, O.; Tarasiuk, W.; Tsybrii, Y.; Nosko, A.; Senatore, A.; D'Urso, V. Performance of acicular grindable thermocouples for temperature measurements at sliding contacts. *Measurement* **2021**, *181*, 109641, doi: 10.1016/j.measurement.2021.109641.